Optica Applicata, Vol. LVI, No. 1, 2026
DOI: 10.37190/oa/214104

Multi-chromatic reflectance polarimetry for mango storage assessment using liquid crystal polarization rotator imaging system

K.H. NG[1,2], K.S. LIM[1,2,*]

[1] Photonics Research Centre, University of Malaya, Kuala Lumpur 50603, Malaysia

[2] Institute for Advanced Studies, University of Malaya, Kuala Lumpur 50603, Malaysia

[*]Corresponding author: kslim@um.edu.my

In this work, a reflectance polarimetry imaging system based on liquid crystal polarization rotator is proposed for the assessment of ripening process of mangoes. A low-cost voltage-controlled liquid crystal polarization rotator and a wire-grid polarizer were integrated into input ray path of a digital camera, enabling selective acquisition of horizontally or vertically polarized (0° and 90°) input images. Unripe Chokanan mango samples were subjected to the illumination of linearly polarized LED light at different wavelength. Digital images at two polarization states were recorded daily until the mangoes were fully ripened on the eighth day. Average reflectance intensity and Degree of Linear Polarization (DoLP) and the findings indicate the dynamic correlation between the varying reflectance intensity, illumination wavelength and the associated dominant pigments (*e.g.* carotenoids, anthocyanins and chlorophylls) in the fruit epidermis during the ripening process. In addition, the DoLP at different wavelengths have shown different variation characteristics with ripening. Notably, DoLPs at 593 and 660 nm decrease with ripening, due to decreasing moisture content in the fruit epidermis that promises light scattering and depolarization in the epidermis tissues. The study demonstrates the potential of reflectance polarimetry as a non-invasive method for assessing the ripeness and storage condition of fruits.

Keywords: polarimetry, liquid crystal, pigments, imaging system.

1. Introduction

The quality and shelf-life of fruits are critical factors in the agricultural industry, impacting both economic viability and consumer satisfaction [1]. Traditional methods for assessing fruit ripeness often involve destructive testing or subjective visual inspection, which can be inefficient and inconsistent [2]. There is a growing need for non-invasive, objective, and real-time techniques to monitor fruit quality during storage.

Polarimetry, the study of the polarization of light, offers a promising avenue for such non-invasive assessments. The interaction of light with biological tissues, such as fruits, is a complex process encompassing absorption, scattering, and reflection, all of which modify the polarization state of the light captured by a camera. These changes are sensitive to the physicochemical transformations occurring within the fruit during ripening, such as changes in pigment concentration, cellular structure, and water content. Reflectance polarimetry, specifically, measures the polarization state of light reflected from a surface, providing insights into the optical properties and underlying physiological changes of the material.

Prior research on the polarimetric properties of fruit tissue has focused on pears using a 632.8 nm laser [3] and apples illuminated by red (650 nm) and white light sources [4]. Using near-infrared (NIR) spectroscopy and aquaphotomics, the paper [5] investigates how linearly polarized and unpolarized light interact with kiwifruit. The study found that polarized light activates more free water states while unpolarized light activates more bound water states, with these differences likely occurring near the fruit's surface. The fruit's soluble solids content was not a significant factor in these findings. Reference [6] reported an automated imaging bidirectional reflectance distribution function polarimeter successfully demonstrated that cross-polarization effectively removes glare from apples across various cultivars and angles, significantly improving machine vision for fruit quality inspection.

This paper introduces a novel reflectance polarimetry system for mango storage, distinguished by several key innovations: it uniquely expands the observable range to five distinct wavelengths through the integration of a cost-effective, voltage-controlled liquid crystal polarization rotator, thereby eliminating the need for mechanical parts. The research uses this advanced, non-mechanical system to investigate mangoes (chosen for their economic importance) by analysing how the degree of linear polarization (DoLP) and intensity of reflected light, including the interaction of several different wavelengths with various pigments during the ripening process. Further novel contributions include the proposal of a new mathematical model relating DoLP, moisture content, and the transport mean free path. By quantifying these optical parameters over an eight-day storage period, we aim to establish the feasibility of polarimetric imaging as a tool for non-invasively monitoring fruit ripeness and quality, offering a potential alternative to conventional assessment methods.

2. Methods

2.1. Experimental setup

In the experiment, LEDs with central wavelengths of 450, 495, 532, 593, and 660 nm were used as the illumination sources. These specific wavelengths were chosen because they correspond to the absorption spectra of known pigments found in mangoes. First, this light was conditioned by using several layers of optical diffuser plates, fol-

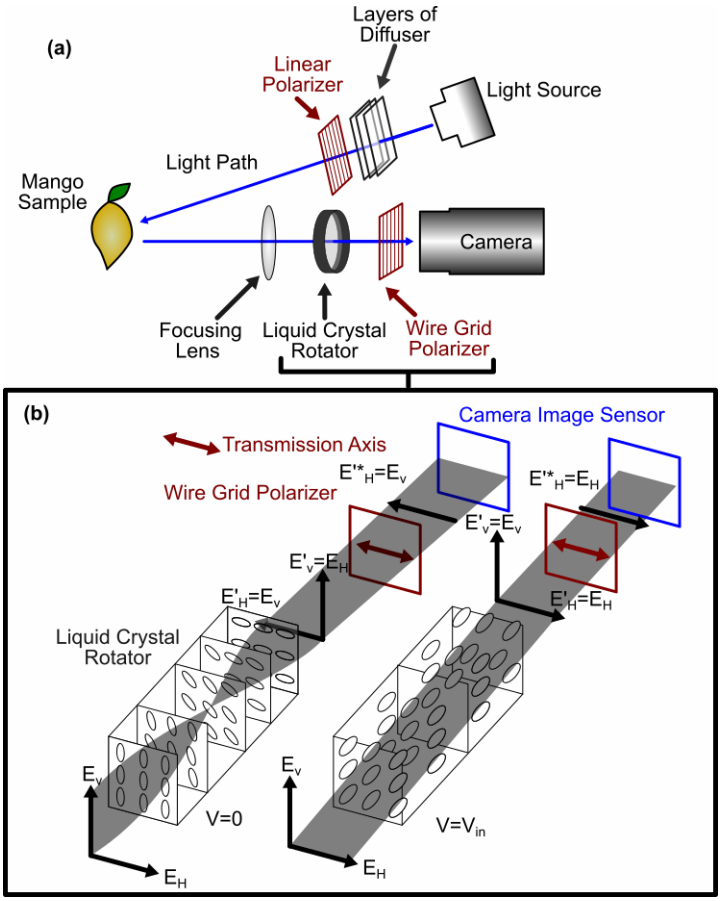

Fig. 1. Illustration of (a) the experimental setup and (b) the liquid crystal polarization rotator imaging system (left: no voltage applied; right: voltage applied). *E* denotes the electric field of the light, with subscripts H and V indicating horizontal and vertical components, respectively. Superscripts ′ and * denote the transmitted electric field after the liquid crystal polarization rotator and the wire grid polarizer, respectively.

lowed by a linear polarizer to produce homogenous linearly polarized light. To eliminate the influence of polarization dependent Fresnel reflection, the light source was positioned adjacent to the imaging camera, thereby minimizing the angle between the light source and the image sensor.

The imaging system comprises a CMOS camera (Hikrobot MV-CU013-A0GC) and a wire grid polarizer positioned directly in front of its image sensor. A low-cost, voltage-controlled liquid crystal polarization rotator (see Fig. 1(a)), made from nematic liquid crystal enclosed within an indium tin oxide (ITO) cell, was integrated into the optical path just before the wire grid polarizer. In the ideal condition (zero applied voltage), the liquid crystal polarization rotator rotates the input polarization plane by 90°.

Specifically, horizontally polarized light is rotated to become vertically polarized, and vertically polarized light is rotated to become horizontally polarized, both with negligible intensity loss. When a voltage of 5 V is applied, the liquid crystal molecules align with the electric field, allowing horizontally polarized light to pass through unchanged. This mechanism enables electronic control over the polarization state—either horizontally or vertically polarized images—by adjusting the applied voltage, while the transmission axis of the wire grid polarizer remains fixed (see Fig. 1(b)).The camera settings were fixated and standardized throughout the experiment to ensure consistency. All automatic features were disabled. The exposure time was set to 300 ms, gain to 0, and red, green, and blue balance ratios were all set to 1024 (corresponding to a ratio of 1.0 [7]).

2.2. Sample preparation and data acquisition

The camera was focused on two unripe Chokanan mango samples room temperature (24 °C) and 60% relative humidity subjected to uniform linear polarized light illumination. For each sample and at each specified wavelength, 8-bit images were recorded at 0° and 90° polarization with respect to the linear polarized light source as shown in Fig. 2.

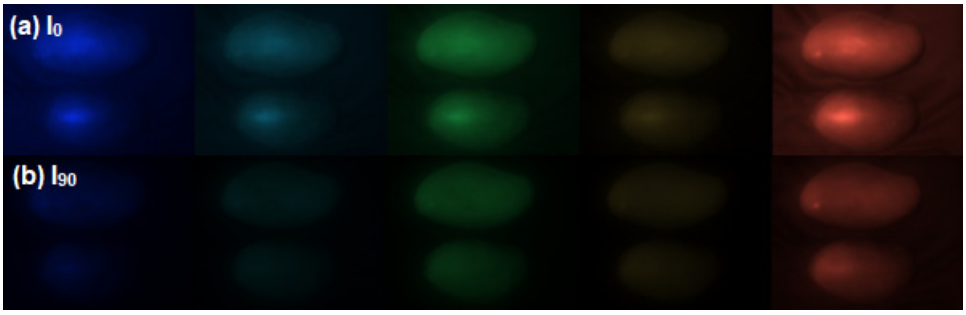

Fig. 2. Images of samples 1 and 2 (a) 0° polarization and (b) 90° polarization at different wavelengths (from left: 450, 495, 532, 593, and 660 nm) on day 1. Image de-mosaicing was performed solely for visual representation and was not applied to the data used for analysis.

Raw image data (prior to de-mosaicing) was processed to extract red, green, and blue pixel values corresponding to specific wavelengths: red pixels for 660 nm, green pixels for 495, 532, and 593 nm, and blue pixels for 450 nm. Particularly, the data for 660 nm are the most significant in terms of intensity changes as shown in Fig. 3. Both captured I_0 and I_{90} images are brighter on day 8 as compared to day 4.

For quantitative analysis, a square region of interest (ROI) was selected for each mango. ROI sizes of 240×240 pixels or 150×150 pixels were chosen based on suitability for each sample (see Fig. 3(c)). Within the ROI, the average intensity and DoLP across the entire ROI were calculated for all wavelengths. Pixels with saturation values (pixel

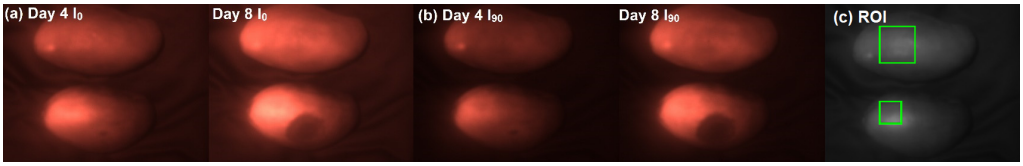

Fig. 3. Images of samples 1 and 2 at wavelength 660 nm (left: day 4 and right: day 8) (a) 0° polarization and (b) 90° polarization. Image de-mosaicing was performed solely for visual representation and was not applied to the data used for analysis. (c) The selected region of interests (ROI) in the images.

Fig. 4. Images of samples 1 and 2 under white light (left: day 1, center: day 4, and right: day 8).

value of 1 (normalized)) or minimum values (pixel value of 0) were excluded from calculations, as they do not provide useful information. Valid pixels value means that pixel value between 0 to 1 (but not include 0 and 1).

Average intensity is calculated using:

$$I'_i = \frac{1}{n}\sum I'_{\text{pix},\, i} \tag{1}$$

where I is average intensity (valid pixels only), subscript i donate the state of polarization 0° and 90°, subscript "pix" donates each valid pixel and n is number of valid pixels in ROI. The superscripts prim indicate the reflected light back into the camera.

Mathematically, average DoLP is given by [8]

$$\text{DoLP} = \frac{s'_1}{s'_0} = \frac{\left|I'_0 - I'_{90}\right|}{I'_0 + I'_{90}} \tag{2}$$

where $s'_0 = I'_0 + I'_{90}$, $s'_1 = I'_0 - I'_{90}$ are Stokes parameters, I'_0 and I'_{90} is average intensity (valid pixel value) in ROI of 0° and 90° polarization light intensity with respected to the linear polarized light source.

This procedure was systematically repeated daily for a period of eight days, continuing until the mango samples reached a ripe state. The rate of change (gradient) and coefficients of determination (R^2) of the average intensity and DoLP are calculated and discussed.

2.3. Empirical model for DoLP

DoLP is strongly influenced by the microstructure of epidermal tissues, as well as by the absorption of the pigments they contain. Additionally, the moisture content within the epidermis plays a significant role in affecting light scattering properties. Based on these factors, an empirical mathematical model for DoLP is proposed:

$$\text{DoLP} = \gamma \exp(-2\alpha l) \tag{3}$$

where γ describes to the moisture factor's effect on DoLP, α is a factor causing depolarization within the sample, and l is the transport mean free path, accounting for scattering, absorption, and reflection from the sample back to the camera. The factor 2 corresponds to both light's travel path into and out of the fruit surface.

Mathematically, transport mean free path can be described by [9]

$$l = \frac{1}{\mu_a + \mu_s} \tag{4}$$

where μ_a is the absorption coefficient and μ_s is the transport scattering coefficient of the tissues. It is intriguing to note that both μ_a and μ_s are wavelength dependant variable associated with the pigments in the epidermal tissues.

2.4. Muller matrix and Lu–Chipman decomposition

In this section, we introduce the perspective of Muller matrix and Lu–Chipman decomposition.

2.4.1. Simplify of Lu–Chipman decomposition

The relation of input light S_{in}, reflected S_{out} Stokes vector and Mueller matrix, M is given by

$$S_{out} = M S_{in} \tag{5}$$

$$\begin{bmatrix} s'_0 \\ s'_1 \\ s'_2 \\ s'_3 \end{bmatrix} = \begin{bmatrix} m_{00} & m_{01} & m_{02} & m_{03} \\ m_{10} & m_{11} & m_{12} & m_{13} \\ m_{20} & m_{21} & m_{22} & m_{23} \\ m_{30} & m_{31} & m_{32} & m_{33} \end{bmatrix} \begin{bmatrix} s_0 \\ s_1 \\ s_2 \\ s_3 \end{bmatrix} \tag{6}$$

Using Lu–Chipman decomposition [10]

$$M = M_\Delta M_R M_D \tag{7}$$

Diattenuator matrix is given by

$$M_{\mathrm{D}} = m_{00}\begin{bmatrix} 1 & D_{\mathrm{H}} & D_{45} & D_{\mathrm{C}} \\ D_{\mathrm{H}} & k_{\mathrm{D}} + (1-k_{\mathrm{D}})\dfrac{D_{\mathrm{H}}^2}{D^2} & (1-k_{\mathrm{D}})\dfrac{D_{\mathrm{H}}D_{45}}{D^2} & (1-k_{\mathrm{D}})\dfrac{D_{\mathrm{H}}D_{\mathrm{C}}}{D^2} \\ D_{45} & (1-k_{\mathrm{D}})\dfrac{D_{45}D_{\mathrm{H}}}{D^2} & k_{\mathrm{D}} + (1-k_{\mathrm{D}})\dfrac{D_{45}^2}{D^2} & (1-k_{\mathrm{D}})\dfrac{D_{45}D_{\mathrm{C}}}{D^2} \\ D_{\mathrm{C}} & (1-k_{\mathrm{D}})\dfrac{D_{\mathrm{C}}D_{\mathrm{H}}}{D^2} & (1-k_{\mathrm{D}})\dfrac{D_{\mathrm{C}}D_{45}}{D^2} & k_{\mathrm{D}} + (1-k_{\mathrm{D}})\dfrac{D_{\mathrm{C}}^2}{D^2} \end{bmatrix} \tag{8}$$

where $\mathbf{D} = \dfrac{1}{m_{00}}\begin{bmatrix} m_{01} \\ m_{02} \\ m_{03} \end{bmatrix} = \begin{bmatrix} D_{\mathrm{H}} \\ D_{45} \\ D_{\mathrm{C}} \end{bmatrix}$, $D = |\mathbf{D}|$ and $k_{\mathrm{D}} = \sqrt{1-D^2}$.

Retarder matrix is given by

$$M_{\mathrm{R}} = \begin{bmatrix} 1 & \mathbf{0}^{\mathrm{T}} \\ \mathbf{0} & m_{\mathrm{R}} \end{bmatrix} \tag{9}$$

where m_{R} is 3×3 submatrix as defined in reference [10].

Depolarizer matrix represents a pure depolarizer, given by:

$$M_{\Delta} = m_{00}\begin{bmatrix} 1 & 0 & 0 & 0 \\ 0 & a & 0 & 0 \\ 0 & 0 & b & 0 \\ 0 & 0 & 0 & c \end{bmatrix} \tag{10}$$

where a, b and c are depolarization parameters for s_1, s_2 and s_3.

In the present study, only one linearly polarized input light source is used and two orthogonal states in the reflection were recorded and assessed. Hence, the diattenuation (9) and depolarizer (11) in the form of 4×4 matrices can be reduced down to 2×2. It is reasonable to assume that the fruit's epidermal tissues are amorphous. This can be attributed to the cuticles, which are the primary component of the exocarp, a hydrophobic layer primarily composed of cutin and hydrophobic intracuticular waxes that are amorphous [11–13]. Cutin does not preferentially absorb light at any polarization state of light. Thus, $D_{\mathrm{H}} = D_{45} = D_{\mathrm{c}} = 0$. The diattenuation matrix becomes

$$M_{\mathrm{D}} = m_{00}\begin{bmatrix}1 & D_{\mathrm{H}}\\ D_{\mathrm{H}} & 1\end{bmatrix} \tag{11}$$

where $D_{\mathrm{H}} = |D|$.

Depolarizer matrix become

$$M_{\Delta} = \begin{bmatrix}1 & 0\\ 0 & a\end{bmatrix} \tag{12}$$

It is safe to assume that the epidermal tissues of the fruit are non-structural and isotropic, it has zero-retardance and the retarder matrix can be expressed as an identity matrix

$$M_{\mathrm{R}} = \mathbf{I} \tag{13}$$

In the present study, Lu–Chipman decomposition (7) can be rewritten as

$$M = M_{\Delta}\mathbf{I}M_{\mathrm{D}} \tag{14}$$

$$M = m_{00}\begin{bmatrix}1 & 0\\ 0 & a\end{bmatrix}\begin{bmatrix}1 & D_{\mathrm{H}}\\ D_{\mathrm{H}} & 1\end{bmatrix} = m_{00}\begin{bmatrix}1 & D_{\mathrm{H}}\\ a\,D_{\mathrm{H}} & a\end{bmatrix} \tag{15}$$

2.4.2. Intensity change over days

In the simplified case for single input linearly polarized light, Eq. (6) can be presented in the form of 2×2 matrix

$$\begin{bmatrix}s_0'\\ s_1'\end{bmatrix} = m_{00}\begin{bmatrix}1 & D_{\mathrm{H}}\\ a\,D_{\mathrm{H}} & a\end{bmatrix}\begin{bmatrix}s_0\\ s_1\end{bmatrix} \tag{16}$$

$$s_0' = m_{00}(s_0 + s_1 D_{\mathrm{H}}) \tag{17}$$

$$s_1' = m_{00}(a\,D_{\mathrm{H}}\,s_0 + a\,s_1) \tag{18}$$

The relationship between s_0, s_1 input light intensities is given by

$$\begin{aligned} s_0' &= m_{00}(I_0 + I_{90}) + m_{00}(I_0 + I_{90})D_{\mathrm{H}}\\ &= m_{00}(1 + D_{\mathrm{H}})I_0 + m_{00}(1 - D_{\mathrm{H}})I_{90} \end{aligned} \tag{19}$$

Assuming there is only one input linearly polarized light source, 0° polarization light I_0 and I_{90}=0. Equation (19) can be further reduced to

$$s'_0 = m_{00}(1 + D_H)I_0 \tag{20}$$

$$I'_0 + I'_{90} = m_{00}(1 + D_H)I_0 = (m_{00} + m_{01})I_0 \tag{21}$$

2.4.3. Depolarization

To continue the effort of simplification, there is an interesting relationship between the depolarization parameter, a and DoLP. For to determine the depolarization parameters a, we start with (18) express s_0, s_1 in intensity, as explained in Section 2.4.2, I_{90}=0. From (18) and (20), (2) can be deduced to

$$\text{DoLP} = \frac{s'_1}{s'_0} = \frac{a(D_H + 1)}{1 + D_H} = a \tag{22}$$

2.5. Spectroscopic analysis

An optical spectrometer was employed to record the diffuse reflectance spectra over the visible region (400 to 700 nm) of the mango samples 1 on day 1 and day 8. Spectroscopic data were subsequently analysed and discussed. Specifically, the spectral difference (change of absorption spectrum) between day 1 and day 8 was calculated and examined (Fig. 5).

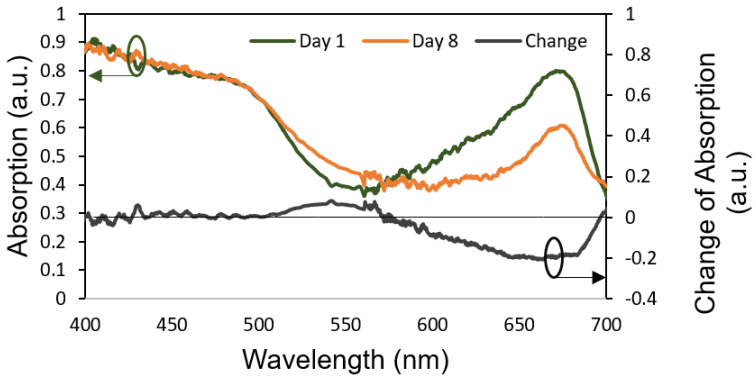

Fig. 5. Absorption spectra of a mango sample 1 for day 1 and 8 and its change in absorption (Abs8 – Abs1).

3. Results and discussion

3.1. Changes in intensity during the storage period

The average intensity values across the region of interest (ROI) were analyzed as a function of storage time. In general, the average intensities for wavelengths of 450, 495, and 532 nm showed a decreasing trend as ripening progressed (see Fig. 6(c)). The decrease observed at 450 and 495 nm is primarily attributed to an increase in carotenoid concentration, as these pigments exhibit peak absorption wavelengths in this spectral

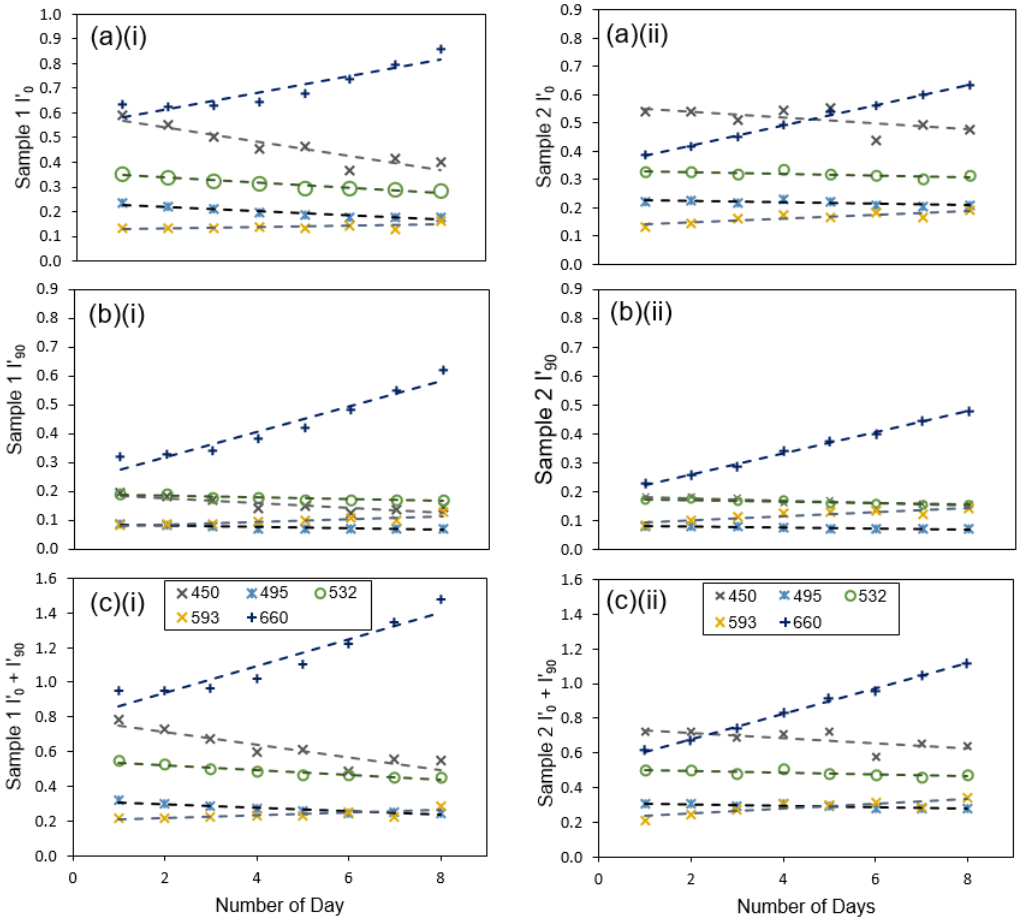

Fig. 6. Normalized intensity of polarization 0° state I'_0 (a), 90° state I'_{90} (b) and sum of both state $(I'_0 + I'_{90})$ (c), over days and its linear fitting for each wavelength for mango sample 1 (i) and 2 (ii).

range [14]. For Mango sample 1, the intensity at these wavelengths became more consistent around day 5, suggesting that the carotenoid content reached a constant state.

Conversely, the average intensities at 593 and 660 nm increased during the ripening process (see Fig. 6(c)). The increment in intensity at 660 nm can be attributed to the decrease in chlorophyll-a, which has an absorption peak near 660 nm [14, 15]. It is commonly known that chlorophyll-a is typically more abundant than chlorophyll-b in mangoes, with a ratio of approximately 3 : 1 [16]. The breakdown of chlorophyll unmasks other pigments, such as carotenoids and anthocyanins. The slight decrease in average intensity at 532 nm is related to the accumulation of anthocyanins in the epidermal tissues, that have an absorption that covers the range of 510–570 nm [17]. Figures 5 and 7(a) suggest that the color shift from green to yellow during ripening (Fig. 4) is a result of chlorophyll degradation. This degradation increases the reflectance of light at 660 nm. The combination of this heightened reflection with the initial green

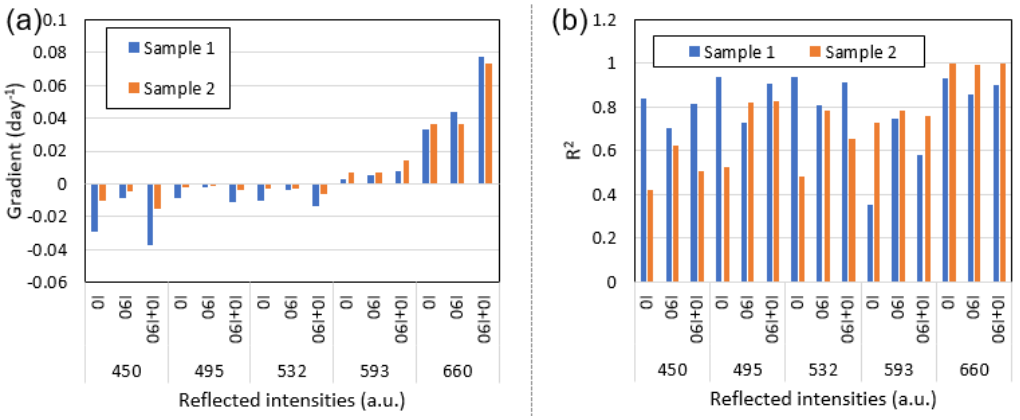

Fig. 7. (a) Bar chart of gradients and coefficients, and (b) determination R^2 for intensity of polarization 0°, 90° and sum change over 8 days for different wavelengths (nm) for samples 1 and 2, obtained via least squares regression.

color of the fruit creates the characteristic yellow color, a phenomenon known as additive color mixing.

Although the intensities for 90° polarization at 593 and 660 nm were less than that for 0° polarization, the rate of change (gradient) was greater for the 90° polarization (Fig. 7(a)). This suggests that 0° polarization is predominantly influenced by specular reflection, whereas 90° polarization light have greater interactions with the pigments in the epidermis before reflection. This phenomenon can also be observed in Fig. 5(a) and (b), which show a relatively low ratio of I'_{90} to I'_0 at shorter wavelengths (450 and 495 nm) compared to longer wavelengths (532, 593, and 660 nm). For example, in day 1, sample 1, the I'_{90}/I'_0 ratios are 0.33 and 0.37 for 450 nm and 495 nm, respectively, in contrast to 0.54, 0.624, and 0.504 for 532 nm, 593 nm, and 660 nm, respectively.

The overall trend in spectrum difference between day 1 and day 8 reveals that absorption increased in the range of 450 to 580 nm (positive change in Fig. 5), corresponding to the observed decrease in average intensity for 450, 495, and 532 nm. Conversely, the absorption decreased in the range of 580 to 690 nm (negative change in Fig. 5), aligning with the increase in average intensity for 593 and 660 nm. This also explains the significantly lower gradient magnitudes (insignificant changes) for 450, 495, and 532 nm intensities compared to 660 nm intensity over time. For instance, the gradient difference between 495 and 660 nm was 86% for sample 1 and 95% for sample 2 (Fig. 7(a)).

From Eq. (21), we conclude that $I'_0 + I'_{90}$ is proportional to I_0, with a proportionality factor of $(m_{00} + m_{01})$. This relationship is evident in Fig. 6(c), where I_0 remains constant daily while the reflected intensity $(I'_0 + I'_{90})$ varies monotonically every day. $m_{00} + m_{01}$ are found to be increasing for 593 and 660 nm and decreasing for 450, 495, and 532 nm over several days for both samples, as explained previously.

3.2. Degree of linear polarization (DoLP) analysis

3.2.1. Changes in DoLP during the storage period

Figure 8 presents the variation of DoLP for different wavelength during the storage period. The average DoLP at 593 and 660 nm generally decrease as the mangoes ripened. This is consistent with the results reported in [3]. This can be observed from the rapid increasing I_{90} (higher gradient) that approaches the I_0 for 593 and 660 nm in the ensuing days (Fig. 6(a,b) and 8(a)). This leads to a smaller numerator $|I_0 - I_{90}|$ in relative to the denominator $|I_0 + I_{90}|$ and produces a lower DoLP. The decrease in DoLP for these wavelengths, coupled with their greater penetration depth (higher reflection, lower absorption, and greater change in absorption as indicated by spectral data), suggests the increased transport mean free path.

It is commonly known that harvested fruits lose water to the ambient over time, Ref. [18] show that Chokanan mango experienced a 2.3% weight loss after two days of storage, reaching the highest rate of 6.98% on the 8th day of ripening. The observed depolarization believed to be related to the decrease in water content over time. When the moisture content in the epidermis tissues is high, the propagation of light in the epidermis experiences less scattering, hence retaining most of its original polarization state or undergoing less depolarization from the multiple scattering events in the tissues. This leads to a higher DoLP and *vice versa*. Another contributing factor to variation of DoLP is the penetration depth, which is inversely related to absorption: higher absorption leads to lower penetration depth, less depolarization, and thus higher DoLP. Conversely, lower absorption leads to greater penetration depth, more depolarization, and lower DoLP.

For 450 and 495 nm, which exhibit high absorption and consequently poor penetration depth and limited light-tissue interaction, no significant observation or correlation could be established from the DoLP data as indicate on it relatively lower

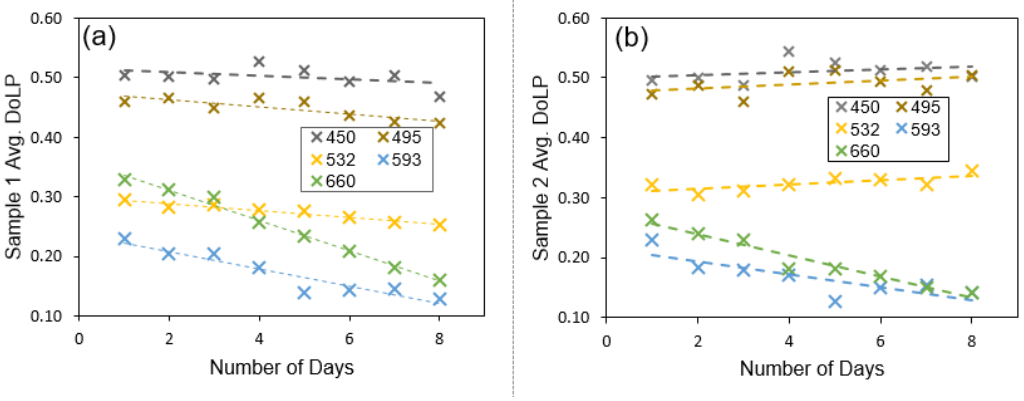

Fig. 8. Degree of linear polarization (DoLP) for mango sample 1 and 2 against storage days for each wavelengths (nm).

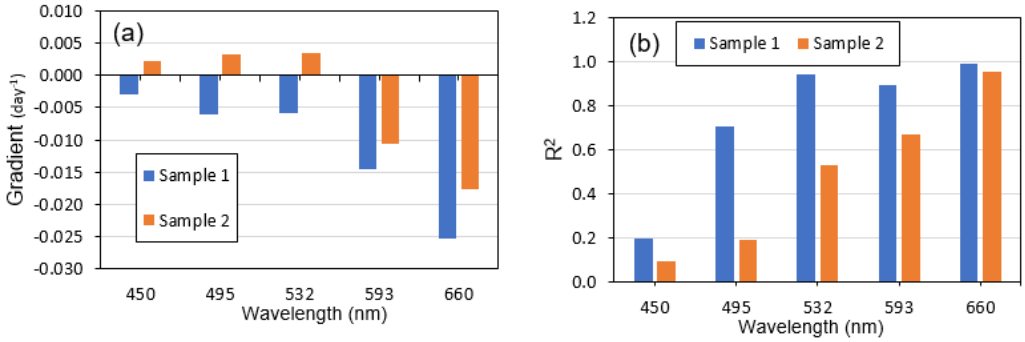

Fig. 9. (a) Gradients and (b) coefficients of determination R^2 for average DoLP over 8 days at different wavelength (nm) for samples 1 and 2.

gradient and R^2 as shown in Fig. 9. This is compounded by the complex pigment changes at 450 nm, involving both decreasing chlorophyll-b and potentially varying rates of carotenoid increase. For 450 and 495 nm, which exhibit high absorption and consequently poor penetration depth and limited light-tissue interaction, no significant observation or correlation could be established from the DoLP data as indicate on it relatively lower gradient and R^2 as shown in Fig. 9. This is compounded by the complex pigment changes at 450 nm, involving both decreasing chlorophyll-b, varying rates of carotenoid increase and loss of water content. This explains the discrepancy in the trends at 450 and 495 nm between sample 1 and sample 2.

The discrepancy in the trends at 532 nm between sample 1 and sample 2 may indicate different rate of change in anthocyanins level between the two samples, as evidenced by a 57% difference in the intensity gradient at 532 nm between sample 1 and sample 2 (see Fig. 7, the $I_0 + I_{90}$ bars at 532 nm).

In general, the DoLP decreased as wavelength increased (from 450 to 593 nm). This is believed to be due to decreasing absorption with increasing wavelength. As absorption decreases, penetration depth increases, leading to more interactions with molecules and thus greater depolarization before reflection, resulting in a lower DoLP.

The 660 nm wavelength is optimal for assessing mango ripeness due to the significant changes it exhibits in both average intensity and degree of linear polarization (DoLP). This phenomenon is a direct result of chlorophyll degradation during the ripening process, which alters light absorption and polarization properties at this wavelength. The use of white light, however, is not ideal because it lacks specificity for a particular pigment.

While conventional colour imaging methods are highly sensitive to light source intensity and the camera's quantum efficiency (QE), polarimetry methods using the degree of linear polarization (DoLP) are significantly less susceptible to these variations. This robustness stems from the DoLP calculation, which involves subtracting two orthogonal polarization states and then normalizing by the total intensity. Ideally, this normalization makes DoLP measurements independent of both the light source inten-

sity and the camera's QE, provided that the signal remains within the sensor's dynamic range (*i.e.*, above the noise floor and below saturation).

3.2.2. Proposed empirical model for DoLP

As detailed in Section 3.2.1, the loss of moisture content (represented by γ in Eq. (4)) within the fruit epidermis contributes to the decrease in DoLP during storage. It is reasonable to assume that this effect applies across all wavelengths examined in this study.

From the absorption and DoLP histogram for day 1, mango sample 1 (Fig. 10), it is evident that wavelengths with higher absorption generally exhibit greater DoLP. This observation aligns with Eq. (5), since the tissue structure remains consistent if we assume the scattering coefficient μ_s and moisture parameter γ are constant for the same day. An increase in absorption coefficient μ_a results in a shorter interaction length l within the tissue, which leads to a larger exponential term $\exp(-2\alpha l)$ and consequently a higher DoLP.

This also explains why the changes in DoLP at shorter wavelengths (450, 495, and 532 nm) (Fig. 9(a)) were less pronounced than those at longer wavelengths (593 and 660 nm) over the storage period.

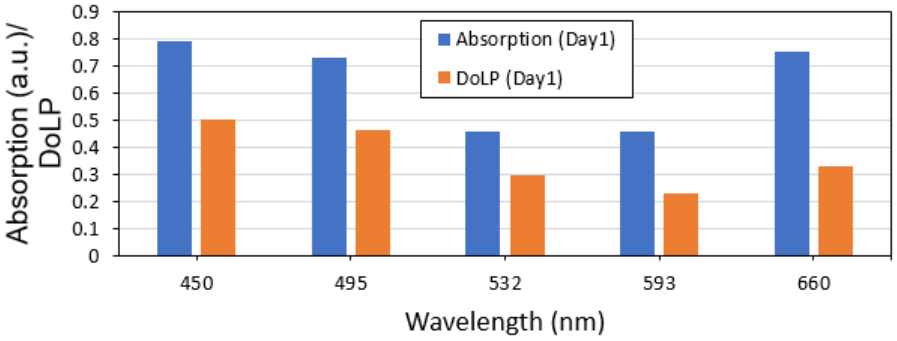

Fig. 10. Absorption and degree of linear polarization (DoLP) for mango sample 1 on day 1.

3.3. Theoretical resolution limit

For an 8-bit image, with $2^8 = 256$ possible pixel values, the theoretical minimum resolution for normalized intensity (where 1 is maximum/saturated and 0 is no signal) is $\Delta I_{res} = 1/255 \approx 0.004$. Any difference smaller than 0.004 is considered indistinguishable.

To determine the theoretical minimum resolution of DoLP, we use the formula:

$$\mathrm{Res}_{\mathrm{DoLP}} = \frac{I_{\max} - I_{\min}}{I_{\max} + I_{\min}} \tag{23}$$

where I_{max} and I_{min} are the maximum and minimum intensities produced by the polarization state, respectively. Considering that possible intensity values are integers be-

tween 0 and 255, the smallest possible non-zero difference in the numerator ($I_{max} - I_{min}$) is 1. The smallest non-zero DoLP difference occurs when the denominator is maximized, which happens when $I_{max} = 255$ and $I_{min} = 254$, yielding a denominator of 509. Therefore, the theoretical minimum resolution (smallest distinguishable step) for DoLP is $1/509 \approx 0.00196$ or ~0.2%. In this study, the observed changes in both intensity and DoLP were generally significantly larger than this theoretical minimum resolution.

3.4. Limitations

It is important to note that only trends in the intensity of each wavelength can be objectively discussed due to inherent limitations of the optical setup. The sensitivity of the system varies across different wavelengths due to system losses and the quantum efficiency (QE) of the camera. For example, the QE for our camera is generally higher near 450 nm (for blue pixels) and lower near 495 nm (for green pixels) [19], which limits the dynamic range of the measurements. However, for the DoLP term, since it is normalized by total intensity, it can be discussed objectively across different wavelengths.

We noted that the polarization extinction ratio (PER) may be wavelength-dependent owing to the use of a liquid crystal rotator. Nonetheless, the measured PER was found to range from 10:1 to 30:1 across the studied wavelengths. This range is acceptable for most industrial use cases, with the resulting visual differentiation as depicted in Fig. 2.

4. Conclusion

This study has demonstrated the polarimetric imaging system based on liquid crystal polarization rotator for observing the ripening process of Chokanan mangoes over an eight-day storage period. The system effectively captured changes in light intensity and the degree of linear polarization (DoLP) at various wavelengths, providing valuable insights into the internal biochemical and physical transformations occurring during ripening.

Our findings reveal distinct trends in light intensity at different wavelengths, correlating with known pigment changes in mangoes. Decreases in intensity at 450, 495, and 532 nm were linked to increased carotenoid concentration in the epidermis tissues and unmasking of anthocyanins, while the increments at 593 and 660 nm were attributed to the diminishing chlorophyll. Furthermore, the systematic decrease in DoLP at 593 and 660 nm as mangoes ripened suggests increased light-tissue interactions due to changes in internal structure and, notably, a decrease in moisture content. The proposed empirical model for DoLP, incorporating factors related to moisture, depolarization, and transport mean free path, aligns with the observed data, particularly emphasizing the significant impact of moisture loss to depolarization.

While shorter wavelengths (450, 495, and 532 nm) show less significant changes in DoLP over time due to limited light penetration, the pronounced changes observed

at longer wavelengths (593 and 660 nm) highlight their potential for effective ripeness monitoring. 660 nm light is found to be most suitable for reflectance polarimetry mango storage assessment. The study underscores the sensitivity of polarized light to subtle physiological changes in fruit, suggesting that reflectance polarimetry is a promising non-invasive technique for real-time assessment of fruit quality and storage conditions.

Declaration of competing interest
The authors declare no competing interests.

References

[1] Gollin D., Parente S., Rogerson R., *The role of agriculture in development*, American Economic Review **92**(2), 2002: 160-164. https://doi.org/10.1257/000282802320189177
[2] Rizzo M., Marcuzzo M., Zangari A., Gasparetto A., Albarelli A., *Fruit ripeness classification: A survey*, Artificial Intelligence in Agriculture **7**, 2023: 44-57. https://doi.org/10.1016/j.aiia.2023.02.004
[3] Nassif R., Pellen F., Magné C., Le Jeune B., Le Brun G., Abboud M., *Scattering through fruits during ripening: Laser speckle technique correlated to biochemical and fluorescence measurements*, Optics Express **20**(21), 2012: 23887-23897. https://doi.org/10.1364/OE.20.023887
[4] Sarkar M., Gupta N., Assaad M., *Monitoring of fruit freshness using phase information in polarization reflectance spectroscopy*, Applied Optics **58**(23), 2019: 6396-6405. https://doi.org/10.1364/AO.58.006396
[5] Rajkumar D., Künnemeyer R., Kaur H., Longdell J., McGlone A., *Interactions of linearly polarized and unpolarized light on kiwifruit using aquaphotomics*, Molecules **27**(2), 2022: 494. https://doi.org/10.3390/molecules27020494
[6] Boyer J., Keresztes J.C., Saeys W., Koshel J., *An automated imaging BRDF polarimeter for fruit quality inspection*, Proceedings of the SPIE, Vol. 9948, Novel Optical Systems Design and Optimization XIX, 2016: 99481G. https://doi.org/10.1117/12.2239008
[7] Hikrobotics GigE Area Scan Camera User Manual, V3.4.9, 20200422
[8] Solomon J.E., *Polarization imaging*, Applied Optics **20**(9), 1981: 1537-1544. https://doi.org/10.1364/ao.20.001537
[9] Wang L.V., Wu H.-I., *Biomedical Optics: Principles and Imaging*, Chapter 5, Wiley, 2007: 83-118.
[10] Lu S.-Y., Chipman R.A., *Interpretation of Mueller matrices based on polar decomposition*, Journal of the Optical Society of America A **13**(5), 1996: 1106-1113. https://doi.org/10.1364/josaa.13.001106
[11] Tessmer M.A., Ribeiro B.G., Kluge R.A., Salvador A., Appezzato-da-Glória B., *Characterization of the epidermis and cuticle of the cashew pseudofruit during its development and maturation*, Plants, **12**(2), 2023: 293. https://doi.org/10.3390/plants12020293
[12] Tafolla-Arellano J.C., Zheng Y., Sun H., Jiao C., Ruiz-May E., Hernández-Oñate M.A., González-León A., Báez-Sañudo R., Fei Z., Domozych D., Rose J.K.C., Tiznado-Hernández M.E., *Transcriptome analysis of mango* (Mangifera indica L.) *fruit epidermal peel to identify putative cuticle-associated genes*. Scientific Reports, **7**(1), 2017: 46163. https://doi.org/10.1038/srep46163
[13] Yeats T.H., Rose J.K.C., *The formation and function of plant cuticles*, Plant Physiology **163**(1), 2013: 5-20. https://doi.org/10.1104/pp.113.222737
[14] Guidi L., Tattini M., Landi M., *How does chloroplast protect chlorophyll against excessive light?*, [In] *Chlorophyll*, InTech, 2017. https://doi.org/10.5772/67887
[15] Zscheile F.P., Comar C.L., *Influence of preparative procedure on the purity of chlorophyll components as shown by absorption spectra*, Botanical Gazette **102**(3), 1941: 463-481. https://doi.org/10.1086/334981
[16] Lee J., Schwartz S., *Pigments in Plant Foods: Handbook of Food Science, Technology and Engineering*, CRC Taylor, 2006.

[17] Setareh Parisa, Heidari Reza, Ghasemifar Elham, Jamei Rashid, *Effect of heating, UV irradiation and pH on stability of the anthocyanin copigment complex*. Pakistan Journal of Biological Sciences, **10**(2), 2007: 267-272. https://doi.org/10.3923/pjbs.2007.267.272
[18] Lawson T., Lycett G.W., Ali A., Chin C.F., *Characterization of Southeast Asia mangoes* (Mangifera indica L) *according to their physicochemical attributes*, Scientia Horticulturae **243**, 2019: 189-196. https://doi.org/10.1016/j.scienta.2018.08.014
[19] Hikrobot. MV-CU013-A0GM/GC CMOS GigE Area Scan Camera Datasheet.

Received September 15, 2025
in revised form October 28, 2025